Journal of Power Sources 183 (2008) 590–594

Contents lists available at ScienceDirect

Journal of Power Sources

journal homepage: www.elsevier.com/locate/jpowsour

Short communication

Electrochemical characterisation of air electrodes based on $La_{0.6}Sr_{0.4}CoO_3$ and carbon nanotubes

Doreen Thiele*, Andreas Züttel

Empa, Swiss Federal Laboratories for Materials Testing and Research, Laboratory for Hydrogen & Energy, Überlandstrasse 129, CH-8600 Dübendorf, Switzerland

ARTICLE INFO

Article history:
Received 27 February 2008
Received in revised form 14 May 2008
Accepted 17 May 2008
Available online 23 May 2008

Keywords:
Oxygen reduction reaction
Alkaline
Carbon nanotube
Perovskite

ABSTRACT

The efficiency of fuel cells suffers from the high activation polarisation at the cathode, where the oxygen reduction reaction takes place. In order to improve the performance, air electrodes composed of carbon nanotubes (CNTs) and the perovskite $La_{0.6}Sr_{0.4}CoO_3$ are produced by two different methods and investigated. In the first method CNTs are directly grown on the perovskite and in the second method CNTs and perovskite are combined by ultrasonic mixing. Their catalytic activity towards oxygen reduction in alkaline solution is evaluated by polarisation curves and electrochemical impedance spectroscopy. Best performance shows the electrode composed of 25 wt% CNTs, 55 wt% $La_{0.6}Sr_{0.4}CoO_3$ and 20 wt% PTFE as binder, produced by ultrasonic mixing. The Nyquist plot of this electrode displays two potential-dependent semicircles, accounting for processes on the catalyst surface and for processes depending on the morphology of the electrode.

1. Introduction

Fuel cells are an environmentally friendly and efficient energy conversion device. Many research efforts are going on to understand the factors (e.g. operating conditions, structure and composition of the electrodes) which mainly affect the performance of a fuel cell in order to optimize these systems successively. Still one major problem is the loss of efficiency due to the high activation polarisation at the cathode where the oxygen reduction reaction occurs. The electrode material commonly used today is platinum on a carbon support. Norskov et al. [1] calculated the free energy of the intermediate species of the oxygen reduction on Pt(1 1 1) on the basis of density functional theory (DFT) and constructed the free energy diagram at several electrode potentials. It was shown that the fuel cell cannot deliver 1.23 V, because then adsorbed oxygen tends to be so stable that proton and electron transfer becomes impossible. By lowering the potential, the stability of oxygen decreases and the reaction may proceed. Furthermore, it was shown that the oxygen binding energy depends on the oxygen coverage and also the OH binding energies on the catalyst play a key role. It was stated that it is possible that a class of catalysts exists where oxygen and OH binding energies on the catalyst are more suitable for the oxygen reduction reaction to occur than in the case of platinum.

The gas diffusion electrode is best described by the thin-film flooded agglomerate model of Raistrick [2,3]. Catalyst and support form porous aggregates which are flooded with the electrolyte. The catalyst agglomerates are kept together by the Teflon binder, which creates hydrophobic gas channels. As current is drawn from the electrode, reactant gas diffuses through the channels, dissolves in the film surrounding the agglomerates and, after diffusing a certain distance, reacts on the three-phase boundary (gas, catalyst, electrolyte).

Therefore, the morphology of the electrode is essential apart from the catalytically active material. It is important to generate a large three-phase boundary by having a carrier on which highly dispersed electrocatalysts are supported. The electrode should have a pore structure and hydrophobic nature of pore surface in order to enable the formation of a highly reactive three phase boundary to create an interface where catalyst, electrolyte and oxygen contact effectively with each other [4].

Starting from the consideration of an active catalyst and a superior morphology of the electrode, we use perovskites as catalyst and carbon nanotubes (CNTs) as support for air electrodes in this work.

It was shown that the use of carbon nanotubes leads to a better dispersion of the catalyst on the support, which in turn leads to a better utilisation of the catalyst compared to activated carbons [5–8]. Carbon nanotubes are a promising support material as they exhibit a high specific surface, chemical stability and a nanosized pore structure.

Perovskites have a high oxygen coverage on the surface and a coverage-dependent binding energy for oxygen. They can release

* Corresponding author. Tel.: +41 44 823 4082; fax: +41 44 823 4022.
E-mail address: doreen.thiele@unifr.ch (D. Thiele).

0378-7753/$ – see front matter © 2008 Elsevier B.V. All rights reserved.
doi:10.1016/j.jpowsour.2008.05.042

and take up oxygen in a reversible way [9]. The general formula of perovskites is ABO_3, whereby the B ions are catalytically active 3d, 4d or 5d transition metal ions. The valence state of the B ion is varied by partial substitution of the A ion [10]. In 1970 Meadowcroft [11] described the use of perovskites in zinc air batteries for the first time. It was pointed out that doping of $LaCoO_3$ with Sr increases the conductivity compared to the undoped material. Perovskites are also reported as electrode materials in solid oxide fuel cells (SOFC) [12,13].

We combine CNTs and the perovskite $La_{0.6}Sr_{0.4}CoO_3$ to air electrodes by two different routes and compare them regarding their catalytic activity:

(1) The carbon nanotubes are grown on the perovskite. The idea behind is that the CNTs act as additional gas channel to the hydrophobic network formed by the PTFE and guides the gas directly to the perovskite to create highly active three phase boundary sites.
(2) We simply mix the carbon nanotubes and the perovskite ultrasonically in order to distribute the perovskite between the CNTs.

Electrochemical impedance spectroscopy is a useful tool to shed light on the processes occurring on such electrodes. Also changes in the electrode impedance during their use can be resolved. In this work impedance spectra of electrodes with different catalyst loadings are compared and differences of the ongoing processes in the different electrodes are stressed.

2. Experimental

2.1. Manufacturing of the electrodes

$La_{0.6}Sr_{0.4}CoO_3$ was delivered from Empa, Laboratory for High Performance Ceramics.

The CNTs were produced by fluidized-bed chemical vapour deposition (CVD) [14]. As substrate powder for the CNT synthesis MgO [14] or $La_{0.6}Sr_{0.4}CoO_3$ [15], both impregnated with a $Fe(NO_3)_3$ solution, was used. In case of using MgO, the iron ratio in the precursor powder was 5 wt% and the synthesis temperature was 600 °C. These conditions lead to multi-wall carbon nanotubes with a high BET surface [14]. The MgO substrate was removed after synthesis by a HCl treatment. In case of using $La_{0.6}Sr_{0.4}CoO_3$, the iron ratio in the precursor powder was 16.7 wt% and the synthesis temperature was 675 °C. After synthesis, no purification step followed.

CNT/$La_{0.6}Sr_{0.4}CoO_3$ electrodes with different compositions, as shown in Table 1, were manufactured as follows. CNTs, $La_{0.6}Sr_{0.4}CoO_3$, PTFE dispersion and distilled water were mixed ultrasonically for 1 h. The mixtures were dried for 18 h at 60 °C under air and then heated to 350 °C for 2 h to fix the PTFE onto the carbon surface. 0.04 g of the resulting powder was mixed with 0.16 g petroleum (Petroleum special, bp 180–220 °C, Fluka) to make a paste, which was spread onto a round piece (24 mm in diameter) of teflonized Toray Carbon Paper TP-090T (QuinTech), serving as gas diffusion layer. The two layers, catalytic active layer and gas diffusion layer, were pressed together and heated to 320 °C for 1 h. And the electrode is finished.

The PTFE content was kept constant at 20 wt% in all electrodes. Three electrodes with different ratios of purified CNTs and $La_{0.6}Sr_{0.4}CoO_3$ (Table 1, electrode 2–4) were produced. One electrode was made with the CNTs grown on the perovskite (electrode 1). For comparison one electrode was manufactured with acetylene black (Alfa Aesar) instead of CNTs (electrode 5) and another electrode consisted only of CNTs (electrode 6).

Table 1
Composition of different electrodes

Electrode	Composition
1	80 wt% CNTs/$La_{0.6}Sr_{0.4}CoO_3$–20 wt% PTFE
2	55 wt% CNTs–25 wt% $La_{0.6}Sr_{0.4}CoO_3$–20 wt% PTFE
3	40 wt% CNTs–40 wt% $La_{0.6}Sr_{0.4}CoO_3$–20 wt% PTFE
4	25 wt% CNTs–55 wt% $La_{0.6}Sr_{0.4}CoO_3$–20 wt% PTFE
5	40 wt% AB[a]–40 wt% $La_{0.6}Sr_{0.4}CoO_3$–20 wt% PTFE
6	80 wt% CNTs–20 wt% PTFE

[a] Acetylene black.

2.2. Electrochemical setup

The electrochemical measurements were conducted with a ZAHNER IM6eX electrochemical work station. A three-electrode arrangement was chosen: the to be investigated electrode foil, which was pressed against a contact plate in the holder, served as working electrode. The geometrical active area of the electrode was 0.785 cm^2. The back side (Toray Carbon Paper) was purged with air or oxygen and the catalytic active side was in contact with the electrolyte. The reference electrode was a Hg/HgO electrode (Radiometer Analytical) in a Haber–Luggin capillary and the counter electrode was a Pt disk (Radiometer Analytical). All measurements were carried out in 6 M KOH (Aldrich) at room temperature.

Steady-state current–potential curves were measured from −0.4 to 0.8 V vs. Hg/HgO. The electrochemical impedance spectra were recorded in the frequency range of 100 mHz to 100 kHz. It was measured in the galvanostatic mode, the ac-amplitude was about 10% of the dc-signal. New electrodes as well as the same electrodes aged by cyclic voltammetry were investigated by means of electrochemical impedance spectroscopy. The obtained spectra were fitted with a least squares fitting program (SIM).

2.3. Additional techniques for characterisation

The electrode morphology was studied by scanning electron microscopy (SEM, Hitachi S-4800). The specific surface area of the CNTs and acetylene black were determined by the BET method (Belsorp-Max, Bel, Japan).

3. Results and discussion

3.1. Steady state

Fig. 1 shows the steady state current–potential curves of the different electrodes, measured under air flow. Electrodes, consisting of CNTs and the perovskites, exhibit a smaller polarisation, and therefore a better performance, for the oxygen reduction reaction than electrode 6 containing only CNTs. Especially, in the inset of Fig. 1, we can see that electrode 6 exhibits the largest activation polarisation in the low current density region of all investigated electrodes. This indicates that $La_{0.6}Sr_{0.4}CoO_3$ has a catalytic activity for the oxygen reduction reaction. Also visible in the inset, the electrode with 55 wt% perovskite has the lowest activation polarisation followed by the electrode with 40 wt% perovskite, followed by the electrode with 25 wt% perovskite. The higher the amount of perovskite in the electrode is, the lower the activation polarisation is. This is an additional indication for the catalytic activity of the perovskite. The electrode with the CNTs grown on the perovskite is as good as the electrode with 25 wt% perovskite produced by ultrasonic mixing in the low current density region.

At higher current densities, that means at higher reaction rates, the impact of the morphology of the electrode becomes larger. Oxygen has to reach an active three phase boundary site fast enough to

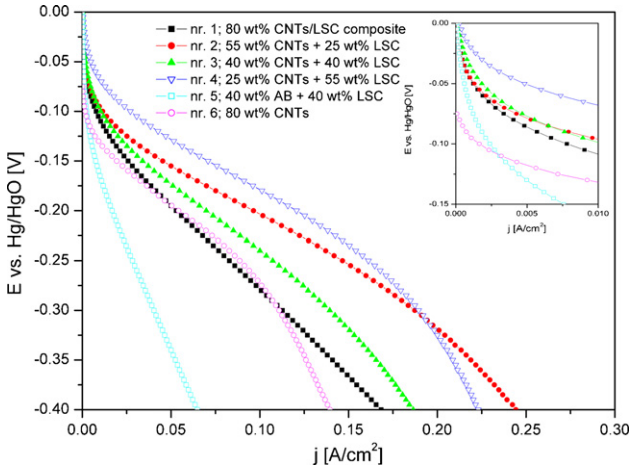

Fig. 1. Steady state current–potential curves of the electrodes summarized in Table 1 (LSC = $La_{0.6}Sr_{0.4}CoO_3$, AB = acetylene black), measured with air.

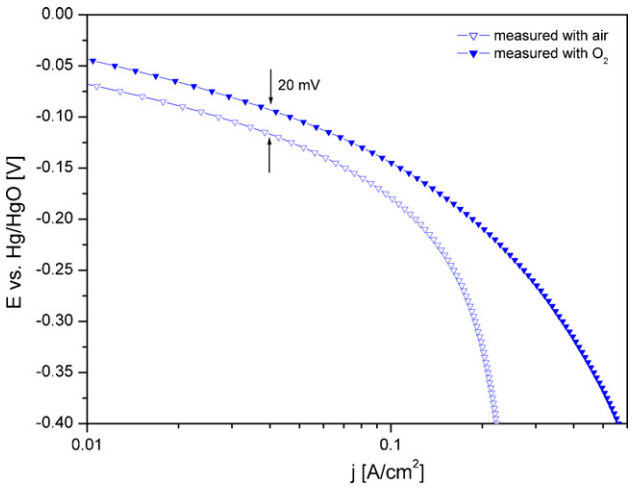

Fig. 2. Steady state current–potential curves of electrode 4, composed of 25 wt% CNTs and 55 wt% $La_{0.6}Sr_{0.4}CoO_3$, measured with air and oxygen.

maintain the reaction. Electrode 5 with acetylene black instead of carbon nanotubes shows then the worst performance. This result can be ascribed to the low specific surface area of acetylene black (62 $m^2\,g^{-1}$) compared to CNTs (440 $m^2\,g^{-1}$). The catalyst is less effective dispersed on acetylene black. Furthermore, the electrodes, synthesized by mixing CNTs and $La_{0.6}Sr_{0.4}CoO_3$, display a better performance (smaller polarisation) than electrode 1 consisting of the CNTs grown on the perovskite. Different aspects contribute to this result. (1) The not purified CNT/perovskite composite contains also amorphous carbon and diverse nanoparticles as by-product of the CNT synthesis. This material has with 62 $m^2\,g^{-1}$ a much lower specific surface area than the purified CNTs (440 $m^2\,g^{-1}$), grown on MgO, for preparing electrodes by ultrasonic mixing of CNTs and perovskite. (2) By growing the CNTs directly on the perovskite it happens that the perovskite is totally covered by CNTs. Therefore, electrolyte and gas cannot reach the catalyst sites. In total this electrode contains less active three phase boundary sites.

The CNT/perovskite composite and acetylene black have the same specific surface area. But electrode 1, composed of CNTs grown on the perovskite displays a much better performance than electrode 5, containing acetylene black and the perovskite. Acetylene black consists of spherical particles, which form larger dense aggregates. In contrast, the CNTs create a conductive network connecting the perovskite particles.

At very high current densities electrode 2 with the high CNT content becomes better than electrode 4 with the high perovskite content. This can be attributed to the better pore structure of the electrode which is provided by the carbon nanotubes. The oxygen can more easily diffuse to the catalyst sites.

In summary, the best electrode had a composition of 25 wt% CNTs, 55 wt% $La_{0.6}Sr_{0.4}CoO_3$ and 20 wt% PTFE produced by ultrasonic mixing. Only at very high current densities the electrode with 55 wt% CNTs and 25 wt% $La_{0.6}Sr_{0.4}CoO_3$ showed the better performance. This result is different from the findings of Arai et al. [16], who examined electrodes containing Ketjen Black and $La_{0.6}Ca_{0.4}CoO_3$. He showed that the electrode with the highest content of Ketjen Black exhibits the best performance in the whole current region, which was ascribed to the larger surface area for the reduction reaction. Furthermore, Arai et al. [16] studied two different carbon supports, Ketjen Black and graphitized, heat-treated Vulcan with specific surface areas of 1300 and 100 $m^2\,g^{-1}$, respectively. In agreement with our findings, the carbon support with the higher specific surface area delivered the better performance. Similar results concerning the specific surface area of the carbon supports were also found by Park et al. [17] and Sawai and Suzuki [18].

The electrode with the best performance was also measured by purging oxygen to the gas diffusion layer instead of air (Fig. 2). At low current densities the difference in potential was about 20 mV, which corresponds to Nernst law, when the oxygen reduction reaction proceeds via the peroxide pathway. At high current densities the difference was bigger. When air is used, the nitrogen builds up a barrier for the oxygen diffusion, leading to a high diffusion polarisation. This result is also in agreement with findings of Arai et al. [16].

3.2. Electrochemical impedance spectroscopy

Fig. 3 shows the electrochemical impedance spectra of the new electrode 3, consisting of CNTs and $La_{0.6}Sr_{0.4}CoO_3$ in equal amounts, measured under oxygen flow. The Nyquist plot displays two potential-dependent semi-circles, which decrease both with increasing overpotential. These two potential-dependent semi-circles were found for all three electrodes, prepared by mixing different amounts of CNTs and perovskite. According to the theory of the thin-film flooded agglomerate model [3] 3 semi-circles

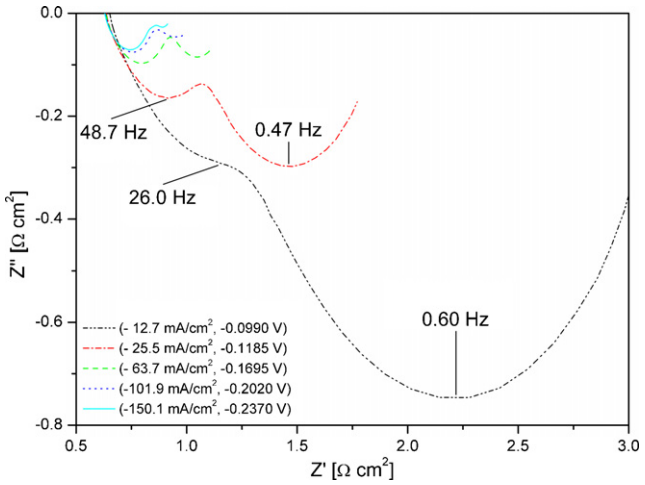

Fig. 3. Nyquist plots of the electrode, composed of 40 wt% CNTs and 40 wt% $La_{0.6}Sr_{0.4}CoO_3$, measured with oxygen at different current densities.

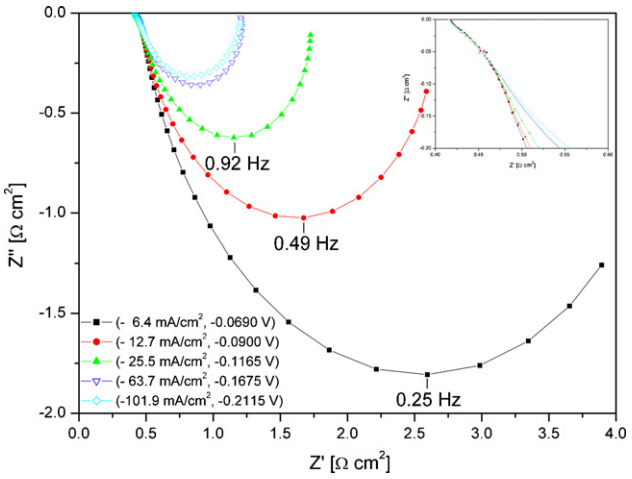

Fig. 4. Nyquist plots of the electrode, composed of 25 wt% CNTs and 55 wt% $La_{0.6}Sr_{0.4}CoO_3$, measured with air at different current densities after aging by cyclic voltammetry.

should be found in the Nyquist plot of porous gas diffusion electrodes; one high frequency arc related to charge transfer processes, one mid-frequency arc related to agglomerate diffusion and one low frequency arc related to diffusion of oxygen through the thin electrolyte film. But this was never observed. Paganin et al. [19], Fischer et al. [20], Huang et al. [21] report about one high frequency potential-independent loop and one low frequency potential-dependent loop. The potential-independent loop is ascribed to distributed resistances inside the catalyst layer. The potential-dependent arc contains information about charge transfer processes, agglomerate diffusion and diffusion through the thin film.

One high frequency potential-independent semi-circle and one low frequency potential-dependent semi-circle, this agrees with the impedance spectra in Fig. 4, we obtained after aging the electrodes by cyclic voltammetry. Cyclic voltammetry leads to cracks in the electrode surface (Fig. 5), resulting in changes of the double layer capacitance. Bultel et al. [22] show by numerical simulations of original models how, depending on the capacitance and other parameters, one potential-dependent arc splits in two arcs, whereby the low frequency arc is related to diffusion and the high frequency arc is related to charge transfer.

The spectra were fitted with an equivalent circuit shown in Fig. 6. The inductance L stands for the mutual induction occurring at high

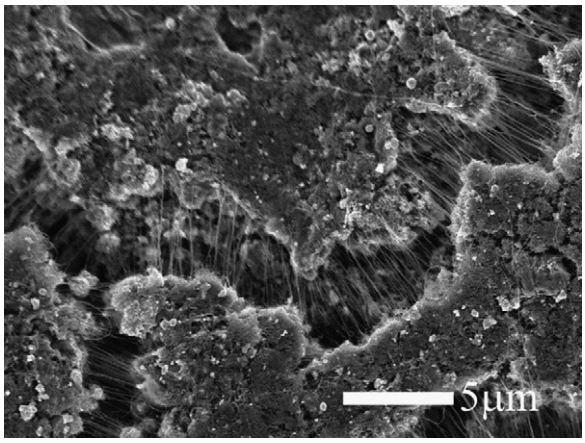

Fig. 5. SEM image of the electrode, composed of 40 wt% CNTs and 40 wt% $La_{0.6}Sr_{0.4}CoO_3$, after cyclic voltammetry.

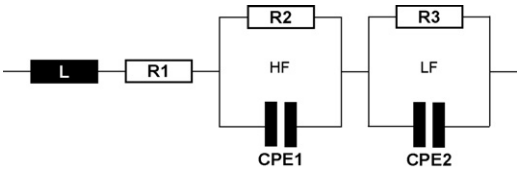

Fig. 6. Scheme of the equivalent circuit.

frequencies. The resistance R_1 represents the sum of electrolyte resistance, contact resistances and cell resistances. It is the high frequency intercept with the real axis in the Nyquist plot. The two semi-circles are described by a series of two parallel *RC* elements, whereby the capacitances are replaced by constant phase elements. It accounts for an only partially charged double layer. The penetration depth of the current into the pores depends on the frequency. At high frequencies, the current travels only through a part of the pores. That means that only a part of the double layer is charged [2]. The impedance of a constant phase element is given by

$$Z_{CPE} = \frac{1}{C_{CPE}(j\omega)^{\varphi}} \quad (1)$$

where C_{CPE} is the distributed capacitance and φ is a constant, $0 < \varphi < 1$. When $\varphi = 1$, C_{CPE} corresponds to the ideal capacitance C. In our case, φ of the high frequency loop was about 0.6, while φ of the low frequency loop was about 0.9.

The high frequency resistance R_2 accounts for processes at the catalyst surface (e.g. charge transfer) and the low frequency resistance R_3 is related to the morphology of the electrodes (e.g. diffusion processes).

The inspection of the low and high frequency resistance against overpotential leads to the conclusion that at low overpotentials the low frequency resistance is bigger than the high frequency resistance and therefore rate determining, while at high overpotentials the high frequency resistance is preponderant; not taking into account, that the low frequency resistance raises again at high overpotentials, when measured with air. The composition of the electrode has an influence on both resistances, R_2 and R_3. R_2 as well as R_3 are smallest when the electrode consists of 25 wt% CNTs and 55 wt% $La_{0.6}Sr_{0.4}CoO_3$ (best electrode 4). The more catalyst in the electrode, the more reaction sites are available. The resistance R_2, related to charge transfer processes, decreases. The high content of perovskite in the electrode has also a positive impact on the morphology of the electrode. The diffusion lengths of oxygen to reach a catalyst particle are shorter, the resistance R_3 decreases.

Also the oxygen content has an influence on both resistances. When measuring with pure oxygen, both resistances are lower. The higher the oxygen content in the feed gas, the more oxygen is delivered to the catalyst sites. The resistance R_2, related to charge transfer processes, decreases. In case of using air, a diffusion barrier for oxygen forms due to a nitrogen cushion. That is why the resistance R_3 is higher with air. When measuring with oxygen, the high frequency loop is shifted to higher frequencies than in case of using air. Higher frequencies mean shorter times. The charge transfer process goes faster if pure oxygen is supplied to the catalyst sites. The higher the overpotential, the faster the charge transfers.

The impedance spectrum of the new electrode 1, made of CNTs grown on the perovskite, shows only one capacitive semi-circle and one inductive loop at low frequencies (Fig. 7). According to Bultel et al. [22], this inductive loop can be ascribed to the concentration impedance of intermediate adsorbed species. In the Nyquist plot of electrode 1 after aging, the inductive loop is not observed anymore in the investigated frequency range. The performance of the electrode becomes slightly better after cyclic voltammetry. A similar behaviour is observed on electrode 5, consisting of acetylene

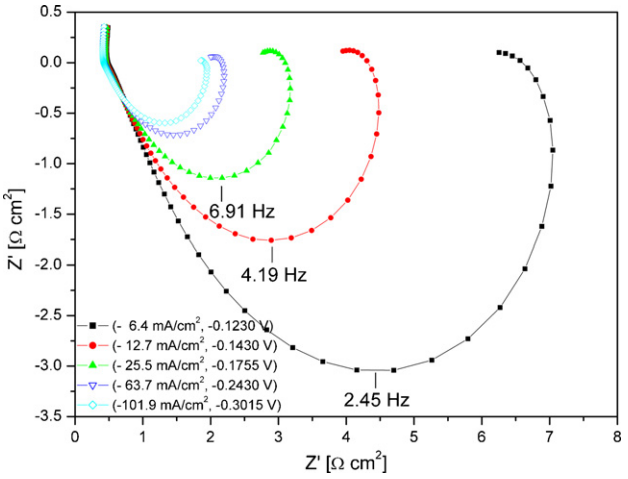

Fig. 7. Nyquist plots of the electrode with the CNTs grown on $La_{0.6}Sr_{0.4}CoO_3$, measured with air at different current densities.

black and $La_{0.6}Sr_{0.4}CoO_3$. The inductive loop disappears after cyclic voltammetry and the performance of the electrode becomes better. Electrode 1 does not only contain CNTs and $La_{0.6}Sr_{0.4}CoO_3$, but also amorphous carbon and other by-products of the CNT synthesis. It is to be likely that the inductive loop is attributed to the carbon support. Species are adsorbed on the carbon support (acetylene black, amorphous carbon) and are removed by cyclic voltammetry. The removing of these adsorbed species leads to a better performance of the electrode.

4. Conclusions

Air electrodes composed of perovskites on a carbon nanotube (CNT) support were produced by two different methods: (A) by growing the CNTs on the perovskite and (B) by ultrasonic mixing of the CNTs and the perovskite. Method B leads to better electrodes for the oxygen reduction reaction because of more active three-phase boundary sites. Electrodes produced by method A contain perovskites which are totally covered by CNTs. Gas and electrolyte cannot reach the catalyst to form an active three phase boundary site. Additionally, these electrodes contain amorphous carbon from the CNT synthesis. Amorphous carbon causes adsorbed intermediates (inductive loop in the Nyquist plot) which lower the performance of the electrode. In the electrochemical impedance spectra of electrodes produced by method B two process are resolved, charge transfer and diffusion.

Future work will be to improve the CNT/perovskite composite, composed of CNTs grown directly on the perovskite. The CNT growth on the perovskite has to be less dense so that gas and electrolyte can reach the catalyst easily. The composite will be purified in order to remove the amorphous carbon and other by-products of the CNT synthesis.

References

[1] J.K. Norskov, J. Rossmeisl, A. Logadottir, L. Lindqvist, J.R. Kitchin, T. Bligaard, H. Jonsson, J. Phys. Chem. B 108 (2004) 17886–17892.
[2] I.D. Raistrick, Electrochem. Acta 35 (1990) 1579–1586.
[3] T.E. Springer, I.D. Raistrick, J. Electrochem. Soc. 136 (1989) 1594–1603.
[4] B. Viswanathan, C. Venkateswara Rao, U.V. Varadaraju, Energy Fuel Res. Signpost (2006), pp. 43–101.
[5] F. Yuan, H. Ryu, Nanotechnology 15 (2004) S596–S602.
[6] T. Matsumoto, T. Komatsu, K. Arai, T. Yamazaki, M. Kijima, H. Shimizu, Y. Takasawa, J. Nakamura, Chem. Commun. (2004) 840–841.
[7] H. Tang, J.H. Chen, Z.P. Huang, D.Z. Wang, Z.F. Ren, L.H. Nie, Y.F. Kuang, S.Z. Yao, Carbon 42 (2004) 191–197.
[8] D. Guo, H. Li, J. Electroanal. Chem. 573 (2004) 197–202.
[9] A. Weidenkaff, Adv. Eng. Mater. 6 (2004) 709–714.
[10] R.J.H. Voorhoeve, D.W. Johnson, J.P. Remeika, P.K. Gallagher, Science 195 (1977) 827–833.
[11] D.B. Meadowcroft, Nature 226 (1970) 847–848.
[12] S.P. Jiang, Solid State Ionics 146 (2002) 1–22.
[13] S.B. Adler, Chem. Rev. 104 (2004) 4791–4843.
[14] Ph. Mauron, Ch. Emmenegger, P. Sudan, P. Wenger, S. Rentsch, A. Züttel, in: T.S. Srivatsan, R.A. Varin (Eds.), Processing and Fabrication of Advanced Materials XI, ASM International, Columbus, OH, USA, 2003, pp. 93–104.
[15] D. Thiele, E. Lopez-Camacho Colmenarejo, B. Grobety, A. Züttel, Diamond Relat. Mater., under review.
[16] H. Arai, S. Müller, O. Haas, J. Electrochem. Soc. 147 (2000) 3587–3591.
[17] K. Park, Y. Sung, S. Han, Y. Yun, T. Hyeeon, J. Phys. Chem. B 108 (2004) 939–944.
[18] K. Sawai, N. Suzuki, Chem. Lett. 33 (2004) 1540–1541.
[19] V.A. Paganin, C.L.F. Oliveira, E.A. Ticianelli, T.E. Springer, E.R. Gonzalez, Electrochim. Acta 43 (1998) 3761–3766.
[20] A. Fischer, J. Jindra, H. Wendt, J. Appl. Electrochem. 28 (1998) 277–282.
[21] H. Huang, W. Zhang, M. Li, Y. Gan, J. Chen, Y. Kuang, J. Colloid Interf. Sci. 284 (2005) 593–599.
[22] Y. Bultel, L. Genies, O. Antoine, P. Ozil, R. Durand, J. Electroanal. Chem. 527 (2002) 143–155.